Hyperfine and magnetic properties of Fe–Cu clusters and Fe precipitates embedded in a Cu matrix

2009 J. Phys.: Condens. Matter 21 506001

(http://iopscience.iop.org/0953-8984/21/50/506001)

J. Phys.: Condens. Matter **21** (2009) 506001 (12pp) doi:10.1088/0953-8984/21/50/506001

Hyperfine and magnetic properties of Fe–Cu clusters and Fe precipitates embedded in a Cu matrix

A B Klautau[1], L M Socolovsky[2], R N Nogueira[3,4] and H M Petrilli[5]

[1] Faculdade de Física, Universidade Federal do Pará, 66075-110, Belém, PA, Brazil
[2] Laboratorio de Sólidos Amorfos, INTECIN, Facultad de Ingeniería, Universidad de Buenos Aires, C1063ACV, Buenos Aires, Argentina
[3] Faculdade Taboão da Serra, 06768-000, Taboão da Serra, SP, Brazil
[4] Universidade Paulista, 06500-000, Santana de Parnaíba, Brazil
[5] Instituto de Física, Universidade de São Paulo, CP 66318, 05315-970 São Paulo, SP, Brazil

E-mail: aklautau@ufpa.br

Received 29 September 2009
Published 23 November 2009
Online at stacks.iop.org/JPhysCM/21/506001

Abstract
Using the first-principles real-space linear muffin-tin orbital method within the atomic sphere approximation (RS-LMTO-ASA) we study hyperfine and local magnetic properties of substituted pure Fe and Fe–Cu clusters in an fcc Cu matrix. Spin and orbital contributions to magnetic moments, hyperfine fields and the Mössbauer isomer shifts at the Fe sites in Fe precipitates and Fe–Cu alloy clusters of sizes up to 60 Fe atoms embedded in the Cu matrix are calculated and the influence of the local environment on these properties is discussed.

(Some figures in this article are in colour only in the electronic version)

1. Introduction

An intense effort has been devoted to understand the unique properties of nanostructured materials. Among the first nanostructured systems ever prepared are Fe–Cu alloys, which are produced by out-of-equilibrium methods [1]. Although Fe and Cu are almost immiscible in the equilibrium state [2], a number of techniques, like sputtering [3–5], fast quenching [6] and mechanical alloying (MA) [7], allow us to exceed the solubility limit by producing metastable solutions in the whole concentration range.

The magnetism of these alloys is known to be a complex subject [8–13]. In bulk, Fe crystallizes in the bcc structure and is ferromagnetic. An fcc phase exists at very high temperatures (γ-Fe) and is non-magnetic [2]. A spiral spin-density wave (SDW) structure of γ-Fe was observed by neutron scattering experiments for samples with pure Fe precipitates in a Cu matrix, where the spherically shaped Fe particles have diameters up to 40 nm [14–16]. Furthermore, the particle size dependence of the SDW state of γ-Fe precipitates in Cu, with wavevector close to the antiferromagnetic 1k-structure, in the limit of very small particles ($\approx$4 nm) [15] was reported. Nevertheless, the magnetic ground state structure of pure γ-Fe is still a matter of intense discussion among the theoretical community [17–27] and the ferromagnetic behavior observed in fcc Fe–Cu alloys [10, 28–30] is also not yet completely understood, and is also a matter of active debate [8, 11, 31–33].

Concerning the structure of these alloys, studies in samples prepared by sputtering [3] and MA [34–36] have established that the Fe–Cu alloys are fcc for less than 60% Fe content. Nevertheless, a question that still remains a subject of debate is what kind of alloy is obtained (homogeneous, nanoclusters, etc) in samples created by different processing techniques [1, 37–39], since different production methods may lead to different alloys. Moreover, some characteristic differences in the hyperfine parameters are observed depending both on the preparation method and on the Cu content. It is remarkable that, despite different concentrations (from 10 to almost 60 at.% of Fe), temperatures and milling conditions, all reported Mössbauer spectroscopy (MS) measurements in samples prepared by MA inferred values in the 20–25 T range for $B_{\rm hf}$s at the Fe sites [28, 40–46]. Nevertheless, in samples made by sputtering and other techniques [3–5] the measured $B_{\rm hf}$s have shown increasing values, following a linear relationship with increasing Fe concentration [3], with small values for low Fe concentration. Also, by comparing Mössbauer isomer shifts (IS) measured in samples made by MA and sputtering, some differences can be observed in the

behavior of the IS when plotted against iron concentration [45]: a decreasing IS tendency with increasing Fe concentration is observed in samples prepared by sputtering [3], but for samples made by MA these values are bounded in a narrow range [45].

In this paper, the first-principles, self-consistent real-space linear muffin-tin orbital method within the atomic sphere approximation (RS-LMTO-ASA) [47, 48] is used to investigate the behavior of Fe–Cu alloy clusters and Fe precipitates, with up to 60 atoms, embedded in a Cu matrix. The main purpose of the present work is to study the hyperfine and magnetic properties of these systems, exploiting the characteristic feature of the RS-LMTO-ASA which allows the *ab initio* study of complex structural situations, in particular the embedding, into an fcc Cu host, of both types of grains: Fe precipitates and Fe–Cu alloy clusters. We also investigate how the hyperfine and magnetic properties evolve as the size of the cluster is increased and we discuss the influence of the local environment on these properties. For this purpose, the spin and orbital local magnetic moments, $B_{\rm hf}$s and ISs at the Fe sites are obtained and analyzed as a function of the Fe content. To gain further insight into the magnetic behavior of Fe clusters, we calculate exchange interactions and magnetic ordering of Fe clusters embedded in Cu. The confrontation of the present $B_{\rm hf}$ and IS theoretical results and values measured at the Fe sites in Fe–Cu systems obtained by different techniques may contribute to the interpretation and better understanding of MS measurements.

2. Theoretical approach

The RS-LMTO-ASA [47, 48] is a parameter-free, fully relativistic, self-consistent method, which follows the steps of the ordinary LMTO-ASA formalism [49], except that it uses the recursion method [50] to solve the eigenvalue problem directly in real space. This method is appropriate for complex metallic systems without periodicity since the computational effort scales linearly with the number of inequivalent atoms and has been successfully applied to study impurities and other defects in metals [48, 51–53], metallic surfaces [54, 55], defects in surfaces [54, 56], multilayers [57] and in the noncollinear RS-LMTO-ASA approach [58]. A detailed description of the method for each situation can be found in the corresponding references cited above. The LMTO-ASA method is a linear method and the solutions are accurate around a given energy E_ν, usually taken at the center of the occupied part of the bands. In the RS-LMTO-ASA scheme we work in the orthogonal representation of the LMTO-ASA formalism and expand the orthogonal Hamiltonian in terms of tight-binding parameters, neglecting terms of the order of $(E - E_\nu)^3$ and higher. In this scheme, the Hamiltonian can be expressed in terms of potential parameters from the tight-binding representation of LMTO-ASA as

$$H = E_\nu + \bar{h} - \bar{h}\bar{o}\bar{h}, \tag{1}$$

where

$$\bar{h} = \bar{C} - E_\nu + \bar{\Delta}^{1/2}\bar{S}\bar{\Delta}^{1/2}. \tag{2}$$

Here the quantities $\bar{C}$, $\bar{\Delta}$ and $\bar{o}$ are potential parameters and $\bar{S}$ is the structural constant in the tight-binding LMTO-ASA representation. These potential parameters are determined self-consistently and are related to solutions of the Schrödinger-like equation inside the Wigner–Seitz sphere associated with each site.

The theoretical magnetic hyperfine field, $B_{\rm hf}$, at a given site **R** can be described as a sum of three terms: Fermi contact $B_{\rm hfc}$, dipolar $B_{\rm dip}$ and orbital $B_{\rm orb}$ contributions. The dipolar contribution $B_{\rm dip}$ is usually very small on transition metal alloys and will not be considered here. In order to evaluate the orbital contributions to the hyperfine fields and the orbital moments, relativistic effects must be taken into account. In the RS-LMTO-ASA the spin–orbit interaction is included in each variational step [59] and orbital polarization (OP) [60] is also included [48, 51]. Details concerning the procedure used here to obtain the orbital moments, $B_{\rm hf}$ and IS can be found elsewhere [48, 51, 61–64].

To simulate the Fe precipitates and the Fe–Cu alloy clusters embedded in a Cu matrix we have used large fcc clusters of ≈12 000 atoms, using the experimental lattice parameter of Cu $a = 3.614$ Å. The clusters embedded in Cu are treated self-consistently as a local perturbation to the surrounding host [47]. In all systems atomic relaxations around the Fe sites embedded in Cu have been neglected. This is a justified approximation when the volume per atom of the impurity in the metal is comparable to that of the host, as in the case of γ-Fe and Cu. Therefore, the present calculations give a reliable theoretical description of the magnetic and hyperfine trends observed in the studied Fe–Cu systems for the chosen lattice parameter. The eigenvalue problem was solved in real space taking 20 levels of recursion and using the Beer–Pettifor terminator [65] to complete the chain. The calculations were performed within the local spin-density approximation (LSDA) using the von Barth–Hedin [66] exchange–correlation functional.

3. Results and discussion

3.1. Studied systems and magnetic structure

We considered two different types of spatial arrangements of the Fe and Cu atoms named here as Fe precipitates and Fe–Cu alloy clusters. The precipitates are substitutional Fe impurity sets embedded in the fcc Cu matrix. These Fe sets are formed by a single Fe atom (an isolated substitutional impurity) or Fe clusters consisting of a central site and successive fcc neighborhoods. We have considered precipitates in which the central Fe site is surrounded by up to four neighboring Fe shells, leading respectively to 1, 13, 43 and 55 Fe atoms in the embedding fcc Cu cluster. These precipitates are labeled here by the number of Fe atoms they contain, with the following notation: Fe1 (isolated impurity), Fe13, Fe19, Fe43 and Fe55. We note that, due to symmetry considerations, all Fe atoms pertaining to a given neighborhood of the central site are equivalent, so we must discuss only a single Fe site per neighborhood. These different Fe sites are denoted here by a subindex according to its corresponding location in a given precipitate, that is: the central Fe is denoted as $\rm Fe_0$ and a typical atom of the nth shell is denoted by $\rm Fe_{\it n}$.

The Fe–Cu alloy clusters are formed by a mixture of Fe and Cu atoms in the substitutional impurity sets (not only by Fe atoms as in the precipitates) embedded in the fcc Cu matrix. We have chosen to consider a group of clusters in which some of the central site neighboring shells are constituted either by Cu or by Fe atoms. We built up three clusters with this type of spatial distribution, which are denoted here by the number of Fe atoms in its composition: Fe36*, Fe37* and Fe60*. For easy reference we introduced the symbol (*) for these alloy clusters. The first one, Fe36*, is formed by a central Cu atom around which complete Fe neighboring shells can be found only in the first and third neighborhoods. In the second, Fe37*, the central position is occupied by an Fe atom, and complete Fe neighboring shells are also placed in the first and third neighborhoods. In the Fe60*, the central atom is Cu and the Fe atoms occupy its first, third and fifth neighborhoods. A detailed structural description of the Fe–Cu alloy clusters and precipitates embedded into fcc Cu studied here is given in table 1. It is worth remarking that we explore, in these cases, the characteristic feature of the RS-LMTO-ASA method which allows us to correctly treat the embedding of both types of grains.

In order to perform our calculations in the context of the complex magnetic behavior exhibited by Fe–Cu alloys and of pure fcc Fe precipitates in Cu, we have considered two different magnetic configurations for the Fe precipitates embedded in Cu: ferromagnetic (FM) and antiferromagnetic (AFM). Among all possible AFM configurations we have chosen the case where all Fe atoms in the same shell of neighbors have parallel spin moments and the AFM coupling is among neighboring shells (denoted here by AFM precipitates). Moreover, for the largest precipitates (Fe43 and Fe55) we have considered a collinear configuration where the moments of Fe atoms in two neighboring inner shells have AFM coupling and the two outermost Fe shells present an FM coupling. These choices are based on previous RS-LMTO-ASA calculations [67] performed for a precipitate with 43 Fe atoms embedded in Cu where, through a comparison among different collinear configurations, it was shown that many different configurations lie very close in energy. For the Fe–Cu alloy clusters embedded in Cu, we have considered the FM arrangement, since this is what has been observed [10, 28–30] in the case of Fe–Cu alloys. Nevertheless, motivated by recent theoretical studies of other Fe-based alloys [26], specifically for the systems denoted by Fe37* and Fe19, we also carried out calculations for the configuration in which the central Fe spin moment is flipped (SF) with respect to all other Fe spin moments.

For Fe13 precipitate embedded in Cu we have found that the FM state has lower energy and the energy difference between the AFM and FM configurations is about 0.3 mRyd/atom. For Fe19 precipitate the FM state is lower in energy than the AFM state (≈2 mRyd/atom) and the SF solution (≈0.2 mRyd/atom). Also, for the Fe37* system the difference in energy between the SF and FM configurations is rather small (≈0.04 mRyd/atom), and may be considered degenerated according to the energy resolution of the RS-LMTO-ASA method.

In agreement with [67], for the precipitate with 43 Fe atoms embedded in Cu we have obtained that the FM configuration is higher in energy compared to other AFM configurations. Moreover, the energy difference between similar antiferromagnetic solutions is shown to be smaller than a few mRyd/atom. As shown in [67], the small difference in energy between AFM solutions is an indication of frustration in the antiferromagnetic interactions. The energy difference between the noncollinear solution and a collinear antiferromagnetic solution is about a few mRyd/atom [67]. The Fe55 precipitate presents an analogous behavior.

In order to discuss on a qualitative level the origin of the calculated magnetic structures, we have calculated exchange interactions J_{ij} for Fe pairs as nearest neighbors (J^{NN}), next-nearest neighbors (J^{NNN}) and next-to-next-nearest neighbors (J^{NNNN}) for all Fe–Cu systems studied here. The exchange interactions have been calculated by using the Liechtenstein *et al* formula [68] as implemented in the RS-LMTO-ASA [69], on a collinear solution. It can be shown that, in general, when biquadratic and higher-order exchanges are relevant, J_{ij} does not give the exchange constant, but actually defines the stability of the ferromagnetic or the antiferromagnetic states [70]. In all cases, when $J > 0$, the spin configuration considered is stable against spin rotations, while for $J < 0$ it is unstable. Moreover, if a canted state exists, both the ferromagnetic and the antiferromagnetic states are unstable (with $J < 0$) [70].

For the Fe13 precipitate embedded in Cu we have found that the exchange interactions between the central Fe atom (Fe_0) and its nearest neighbors in the first shell (Fe_1) are ferromagnetic ($J^{\mathrm{NN}}_{\mathrm{Fe}_0-\mathrm{Fe}_1} = 0.7$ mRyd/atom), as well as the interactions between Fe nearest neighbors and next-nearest neighbors located on the first shell ($J^{\mathrm{NN}}_{\mathrm{Fe}_1-\mathrm{Fe}_1} = 1.3$ mRyd/atom and $J^{\mathrm{NNN}}_{\mathrm{Fe}_1-\mathrm{Fe}_1} = 0.6$ mRyd/atom). On the other hand, the exchange interactions between two Fe positioned as next-to-next-nearest neighbors, in the first shell, are antiferromagnetic ($J^{\mathrm{NNNN}}_{\mathrm{Fe}_1-\mathrm{Fe}_1} = -0.3$ mRyd/atom). Considering the multiplicity of the Fe pairs (n_p) and the fact that the exchange interactions between nearest neighbors and next-nearest neighbors are strongest and ferromagnetic, with a smaller long-range antiferromagnetic interaction, it results in a ferromagnetic state for the Fe13 precipitate. We obtained a similar behavior for the Fe19 precipitate embedded in Cu, in which all Fe atoms as nearest neighbors and next-nearest neighbors present a ferromagnetic coupling ($J^{\mathrm{NN}}_{\mathrm{Fe}_0-\mathrm{Fe}_1} = 0.1$ mRyd/atom, $J^{\mathrm{NN}}_{\mathrm{Fe}_1-\mathrm{Fe}_1} = 0.4$ mRyd/atom, $J^{\mathrm{NN}}_{\mathrm{Fe}_1-\mathrm{Fe}_2} = 1.2$ mRyd/atom, $J^{\mathrm{NNN}}_{\mathrm{Fe}_0-\mathrm{Fe}_2} = 0.9$ mRyd/atom and $J^{\mathrm{NNN}}_{\mathrm{Fe}_1-\mathrm{Fe}_1} = 0.7$ mRyd/atom) and the exchange interactions between two Fe atoms positioned as next-to-next-nearest neighbors are antiferromagnetic ($J^{\mathrm{NNNN}}_{\mathrm{Fe}_1-\mathrm{Fe}_1} = -0.1$ mRyd/atom and $J^{\mathrm{NNNN}}_{\mathrm{Fe}_1-\mathrm{Fe}_2} = -0.2$ mRyd/atom). The exchange interactions between Fe nearest neighbors located on outermost shells (i.e. with larger numbers of Cu first neighbors) are ferromagnetic and the strongest ones. Note that all these calculations have been performed in the ferromagnetic state. We also calculated the J_{ij} between nearest neighbors in the AFM configuration and found that it was unstable. Therefore, the reason for the collinear magnetism of Fe in these systems is due to the absence of competing interactions. In addition, we have found

Table 1. Fe–Cu systems. The clusters embedded in fcc Cu are denoted by the number (N) of Fe atoms they contain: FeN for Fe precipitates and FeN^* for Fe–Cu alloy clusters. Fe_0 (or Cu_0) indicates the central atom in the cluster, while Fe_n (or Cu_n) refers to a typical Fe (or Cu) site in the nth shell around Fe_0 (or Cu_0). The degeneracy of the site is given by d. For each non-equivalent Fe site, nn_{Cu} is the number of Cu first neighbors and nn_{Fe-AFM} is the number of Fe nearest neighbors AFM-coupled to this site. N_{Cu} is the average number of Cu nearest neighbors and N_{Fe-AFM} is the average number of Fe nearest neighbors AFM-coupled to the Fe sites in each cluster.

		FM Fe precipitates						AFM Fe precipitates						Fe–Cu alloy clusters					
		Fe1		Fe13		Fe19		Fe43			Fe55			Fe36*		Fe37*		Fe60*	
n shell	d	Site	nn_{Cu}	Site	nn_{Cu}	Site	nn_{Cu}	Site	nn_{Cu}	nn_{Fe-AFM}	Site	nn_{Cu}	nn_{Fe-AFM}	Site	nn_{Cu}	Site	nn_{Cu}	Site	nn_{Cu}
0	1	Fe_0	12	Fe_0	0	Fe_0	0	Fe_0	0	12	Fe_0	0	12	Cu_0		Fe_0	0	Cu_0	
1	12			Fe_1	7	Fe_1	5	Fe_1	1	3	Fe_1	0	3	Fe_1	4	Fe_1	3	Fe_1	4
2	6					Fe_2	8	Fe_2	4	8	Fe_2	4	8	Cu_2		Cu_2		Cu_2	
3	24							Fe_3	7	1	Fe_3	5	3	Fe_3	8	Fe_3	8	Fe_3	6
4	12										Fe_4	7	5					Cu_4	
5	24																	Fe_5	8
N_{Cu}			12		6.46		5.68		4.74			4.15			6.67		6.16		6.40
N_{Fe-AFM}										2.8			4.1						

Table 2. Spin (m_S) and orbital (m_L) contributions to the magnetic moments (in μ_B units) at the Fe sites, in the absence (no-OP) and including (OP) the orbital polarization [60]. The site notation and N_{Cu} are the same as in table 1. $\bar{M}$ is the average moment per Fe site.

	FM Fe precipitates									AFM Fe precipitates						Fe–Cu alloy clusters								
	Fe1			Fe13			Fe19			Fe43			Fe55			Fe36*			Fe37*			Fe60*		
		m_L			m_L			m_L			m_L			m_L			m_L			m_L			m_L	
	m_S	No-OP	OP	m_S	No-OP	OP	m_S	No-OP	OP	m_S	No-OP	OP	m_S	No-OP	OP	m_S	No-OP	OP	m_S	No-OP	OP	m_S	No-OP	OP
Fe_0	2.54	0.09	0.21	2.23	0.06	0.11	2.25	0.07	0.12	2.26	0.05	0.07	2.23	0.05	0.08				1.93	0.05	0.09			
Fe_1				2.40	0.07	0.11	2.32	0.06	0.10	−1.69	−0.04	−0.07	−1.15	−0.03	−0.06	2.30	0.05	0.08	2.28	0.05	0.08	2.39	0.05	0.08
Fe_2							2.39	0.07	0.12	2.21	0.07	0.14	2.39	0.07	0.11									
Fe_3										−2.31	−0.06	−0.11	−1.89	−0.06	−0.12	2.44	0.06	0.10	2.43	0.06	0.10	2.40	0.05	0.09
Fe_4													2.35	0.08	0.16									
Fe_5																						2.40	0.06	0.10
$\bar{M}$	2.54	0.09	0.21	2.39	0.07	0.11	2.34	0.06	0.11							2.39	0.06	0.10	2.37	0.06	0.10	2.40	0.06	0.09
N_{Cu}		12			6.46			5.68			4.74			4.15			6.67			6.16			6.40	

that the exchange interactions between nearest neighbors and next-nearest neighbors for all Fe–Cu alloy clusters (Fe36*, Fe37* and Fe60*) are ferromagnetic. The small difference in energy between the FM and SF configurations for the Fe37* systems can be understood by the competition between the ferromagnetic coupling of the central Fe atom with its 12 nearest neighbors ($J^{\mathrm{NN}}_{\mathrm{Fe}_0-\mathrm{Fe}_1} = 0.48$ mRyd/atom) and the AFM coupling of the Fe central atom with its 24 next-to-next-nearest neighbors ($J^{\mathrm{NNNN}}_{\mathrm{Fe}_0-\mathrm{Fe}_3} = -0.21$ mRyd/atom). Note that for this system (Fe37*) the central atom has no Fe atom as next-nearest neighbor (see table 1).

In the largest precipitates (Fe43 and Fe55), the exchange interactions are ferromagnetic between both Fe nearest neighbors and next-nearest neighbors, located on either the same or different outermost shells (e.g. $J^{\mathrm{NN}}_{\mathrm{Fe}_2-\mathrm{Fe}_3} = 0.9$ mRyd/atom, $J^{\mathrm{NN}}_{\mathrm{Fe}_3-\mathrm{Fe}_3} = 1.0$ mRyd/atom or $J^{\mathrm{NNN}}_{\mathrm{Fe}_3-\mathrm{Fe}_3} = 0.4$ mRyd/atom for the Fe43 system). For Fe pairs on the same inner shell, the exchange interactions: (i) are weak and ferromagnetic for the nearest neighbors (e.g. $J^{\mathrm{NN}}_{\mathrm{Fe}_1-\mathrm{Fe}_1} = 0.01$ mRyd/atom for the Fe43 precipitate) and (ii) the coupling is found to be neither ferromagnetic nor antiferromagnetic between nearest neighbors located on different inner shells (e.g. for the Fe43 system, $J^{\mathrm{NN}}_{\mathrm{Fe}_0-\mathrm{Fe}_1} = -0.4$ mRyd/atom for calculations performed in the ferromagnetic state and $J^{\mathrm{NN}}_{\mathrm{Fe}_0-\mathrm{Fe}_1} = -0.1$ mRyd/atom for calculations in the antiferromagnetic state). Moreover, the exchange interactions present competing values for more distant pairs, with contributions which approximately cancel each other, analogous to previous theoretical results for pure fcc Fe [25, 26] (e.g. $J^{\mathrm{NNN}}_{\mathrm{Fe}_1-\mathrm{Fe}_1} = 0.35$ mRyd/atom ($n_p = 12$) and $J^{\mathrm{NNNN}}_{\mathrm{Fe}_1-\mathrm{Fe}_1} = -0.17$ mRyd/atom ($n_p = 24$) for the Fe43 precipitate), indicating a probable cause for the complex noncollinear magnetic structure showed in [67].

Concerning the hyperfine interactions, and local magnetic moments, we carried out calculations for collinear configurations of the Fe–Cu systems. Moreover, in order to concentrate on the investigation of the trends, and to study general features of the hyperfine interactions for different magnetic structures and spatial arrangements in Fe–Cu systems, we present results for selected, low energy, FM, SF and AFM states. To better understand the trends in our calculations, we include in table 1 the number of Fe nearest neighbors which are antiferromagnetically coupled ($nn_{\mathrm{Fe-AFM}}$) to the Fe atom at a given site.

3.2. Local magnetic moments

Our results for the spin (m_S) and orbital (m_L) contributions to the magnetic moments at the Fe sites for a selection of collinear magnetic configurations described in section 3.1 are shown in table 2. The calculations were performed in two ways: with (OP) and without (no-OP) the inclusion of orbital polarization [60]. Although the spin moment has been calculated by different *ab initio* methods (for a single Fe in Cu [71], some Fe clusters in Cu [72] and for some Fe–Cu alloys [8]), no systematic study of the orbital moments for Fe and Fe–Cu grains in Cu is available. The values of all orbital moments shown in table 2 are systematically enhanced when OP is included in the calculations, although their magnitudes are very small when compared with the spin moments. On the other hand, as expected, the spin moments are not very sensitive to the inclusion of OP (not shown in table 2). Due to this fact, both ways of calculating m_L lead to the same general scenario. Orbital and spin moments induced at Cu sites in the vicinity of the Fe sites were also calculated. These moments are extremely small (of the order of 0.01 μ_{B} for spin moments and 0.002 μ_{B} for orbital moments) and will not be included in our discussions.

As seen in table 2, the spin moments obtained using the FM configurations of the Fe precipitates vary from 2.5 μ_{B} (Fe impurity in Cu) to values around 2.2 μ_{B} (central Fe sites for the Fe13 precipitates) whereas the orbital moments vary from 0.09 μ_{B} (no-OP) and 0.21 μ_{B} (OP), in the case of the Fe impurity, to values of the order of 0.06 μ_{B} (no-OP) and 0.1 μ_{B} (OP) at the internal Fe sites. A significant variable which can be used to better understand the local magnetic trends is the number of Cu neighbors around each Fe site, nn_{Cu}, given in table 1. From tables 1 and 2 we see that both orbital and spin moments slightly increase as nn_{Cu} increases (with a smaller effect on the already small m_L). For the precipitates this means that the moments increase smoothly as one moves from the center to the Fe/Cu interface where the Fe sites have more Cu neighbors, but these correlations with nn_{Cu} are observed here in all FM cases. We notice that correlations among local magnetic moments and nn_{Cu} have already been observed in different 3d systems [61, 52].

Another interesting issue to be addressed is the magnetic behavior as the Fe clusters in Cu grow in size, going from a single Fe atom to Fe nanoparticles. A relevant quantity in this case is the average magnetic moment ($\bar{M}$) per Fe atom in the embedded cluster, whose spin and orbital contributions are shown in table 2, for the FM systems studied here. We see that the average orbital moments for larger clusters are almost constant with values around 0.06 μ_{B} (no-OP) and 0.10 μ_{B} (OP). Since the spin and orbital moments are correlated with the number of Cu neighbors at each Fe site, we can also expect a correlation between the average moments and the average number of nearest-neighbor Cu (N_{Cu}) per Fe site. One should notice that the quantities nn_{Cu} and N_{Cu} are different. To obtain N_{Cu} in a given system we add nn_{Cu}, from all Fe atoms, and divide the result by the number of Fe atoms in this system. As an example, the Fe19 precipitate has, according to table 1, three different Fe shells: the central Fe_0 has $nn_{\mathrm{Cu}} = 0$; each Fe_1, of the 12 Fe atoms in the first shell, has $nn_{\mathrm{Cu}} = 5$; each Fe_2, of the 6 Fe atoms in the second shell, has $nn_{\mathrm{Cu}} = 8$. Therefore, in this case, $N_{\mathrm{Cu}} = (1\times 0 + 12\times 5 + 6\times 8)/19 = 5.68$. If we plot the results shown in table 2 for the spin and orbital contributions to $\bar{M}$ as a function of N_{Cu}, we see that $\bar{M}$ increases almost monotonically as N_{Cu} increases. We have also calculated the moments for the Fe37* system in the SF configuration, obtaining: $m_S = -2.14$ μ_{B} (Fe_0), $m_S = 2.17$ μ_{B} (Fe_1) and $m_S = 2.43$ μ_{B} (Fe_3), and essentially the same magnitudes for the orbital moments as in the FM configuration.

The analysis of the local spin moments obtained in the AFM configuration, shown in table 2, is more complex. Interestingly, we have verified that two competing mechanisms play the important role in this case: the number of Cu nearest neighbors and the number of antiferromagnetically coupled Fe

Table 3. Calculated core (B_{core}), valence (B_{val}) and orbital (B_{orb}) contributions to the hyperfine fields obtained including (OP) or not (no-OP) orbital polarization [60] at the Fe sites (in teslas). The notation is the same as in table 1.

	FM Fe precipitates												AFM Fe precipitates							
	Fe1				Fe13				Fe19				Fe43				Fe55			
			B_{orb}				B_{orb}				B_{orb}				B_{orb}				B_{orb}	
	B_{core}	B_{val}	No-OP	OP	B_{core}	B_{val}	No-OP	OP	B_{core}	B_{val}	No-OP	OP	B_{core}	B_{val}	No-OP	OP	B_{core}	B_{val}	No-OP	OP
Fe_0	−26.72	14.08	4.32	10.00	−24.20	−5.92	2.80	4.99	−24.31	−5.33	2.99	5.49	−23.03	29.47	2.20	3.49	−22.90	21.04	2.43	3.99
Fe_1					−25.53	3.34	3.03	5.25	−24.88	−0.80	2.76	4.86	18.01	−1.80	−1.85	−3.43	12.07	−2.70	−1.58	−3.09
Fe_2									−25.36	3.19	3.07	5.48	−22.65	23.28	3.30	6.66	−24.65	23.59	3.20	5.56
Fe_3													24.40	−7.94	−2.93	−5.22	19.77	−10.49	−2.96	−5.74
Fe_4																	−24.47	19.74	3.92	8.01

	Fe–Cu alloy clusters															
	Fe36*				Fe37*				Fe60*				SF Fe37*			
			B_{orb}				B_{orb}				B_{orb}				B_{orb}	
OP	B_{core}	B_{val}	No-OP	OP	B_{core}	B_{val}	No-OP	OP	B_{core}	B_{val}	No-OP	OP	B_{core}	B_{val}	No-OP	OP
Fe_0					−21.27	−10.53	2.25	4.00					21.54	−31.06	−2.31	−4.16
Fe_1	−24.71	−1.98	2.10	3.50	−24.52	−2.91	2.09	3.53	−25.67	−1.29	2.31	3.45	−23.25	−0.37	2.02	3.48
Fe_2																
Fe_3	−25.91	5.42	2.89	4.94	−25.90	5.20	2.90	4.95	−25.68	1.39	2.40	3.92	−25.89	5.63	2.89	4.96
Fe_4																
Fe_5									−25.62	3.52	2.77	4.69				

nearest neighbors (table 1). Although we are not able to predict which of these two quantities dictates the local moment at a given site, we clearly see that for the same $nn_{\mathrm{Fe-AFM}}$ the largest m_S magnitude is obtained at the Fe site with larger nn_{Cu}. This can be seen, for example, through the comparison of the m_S results at the Fe_1 site in the Fe43 AFM Fe precipitate (where $nn_{\mathrm{Fe-AFM}} = 3$, $nn_{\mathrm{Cu}} = 1$ and $m_S = -1.69\ \mu_{\mathrm{B}}$) and at the Fe_3 site in the Fe55 AFM Fe precipitate (where $nn_{\mathrm{Fe-AFM}} = 3$, $nn_{\mathrm{Cu}} = 5$ and $m_S = -1.89\ \mu_{\mathrm{B}}$). On the other hand, for sites with the same $nn_{\mathrm{Fe-AFM}}$ and nn_{Cu}, the largest m_S magnitude corresponds to the Fe site with the largest number of Fe second-nearest neighbors. We note that, by construction, these Fe second-nearest neighbors are all ferromagnetically coupled to the site considered in the AFM Fe precipitates. The small orbital moments in the AFM configurations follow the same trend shown by the local spin moments. We notice that the general trends of our results for the local magnetic moment in the AFM configuration are in general agreement with both experimental and theoretical results obtained in [73].

3.3. Hyperfine properties

3.3.1. Hyperfine fields. It is usual to decompose the Fermi contact hyperfine field (B_{hfc}) at 3d probes into a core contribution (B_{core}) from 1s, 2s and 3s core electrons and a valence contribution (B_{val}) associated with the 4s electrons. The calculated B_{core}, B_{val} and orbital (B_{orb}) contributions to the hyperfine fields (B_{hf}) at the Fe sites are shown in table 3. As can be seen from tables 2 and 3, there are appreciable orbital contributions to the magnetic moment and hyperfine field in the case of the Fe impurity in Cu. Although these orbital contributions are smaller for the Fe_0 sites in the larger precipitates, we see that even a relatively small orbital moment yields a meaningful contribution to B_{hf}. As discussed before [63] this is due to the large value of the corresponding orbital hyperfine field proportionality constant for Fe $\alpha_{\mathrm{orb}} = B_{\mathrm{orb}}/m_L$ of around $+45\ \mathrm{T}/\mu_{\mathrm{B}}$ in the no-OP case and $+47\ \mathrm{T}/\mu_{\mathrm{B}}$ when OP is included.

A pronounced decrease in the magnitude of B_{hf} is observed as one moves from the center towards the boundary of the FM Fe precipitates. It is clear that the near presence of Cu atoms tends to lower the magnitude of B_{hf} at the Fe sites in all FM systems studied here; if we plot these B_{hf} as a function of nn_{Cu} we easily see that, in both OP and no-OP cases, B_{hf} become less negative as nn_{Cu} increases. Trying to understand the origin of this decrease in the magnitude of B_{hf} we plot in figure 1(a) the core, valence and orbital contributions to the hyperfine fields as a function of nn_{Cu} in the FM systems. In all FM cases B_{core} is large and negative and changes by not more than 5 T with magnitudes that slightly increase as we go from the center to the outermost shells in the precipitates (see table 3). Comparing the theoretical values presented in tables 2 and 3 we see a hyperfine field constant for the core polarization field given by $\alpha_{\mathrm{core}} = B_{\mathrm{core}}/m_S$, which is around $-11\ \mathrm{T}/\mu_{\mathrm{B}}$ in all FM systems considered here. Therefore, in the FM systems (figure 1(a)) B_{core} increases in magnitude (towards more negative values) with increasing nn_{Cu}, a behavior correlated with the m_S tendencies. Also in the AFM Fe precipitates we observe that B_{core} is proportional to m_S, with almost the same α_{core} but, since the spin moment displays a more complicated behavior (see table 2), there is no

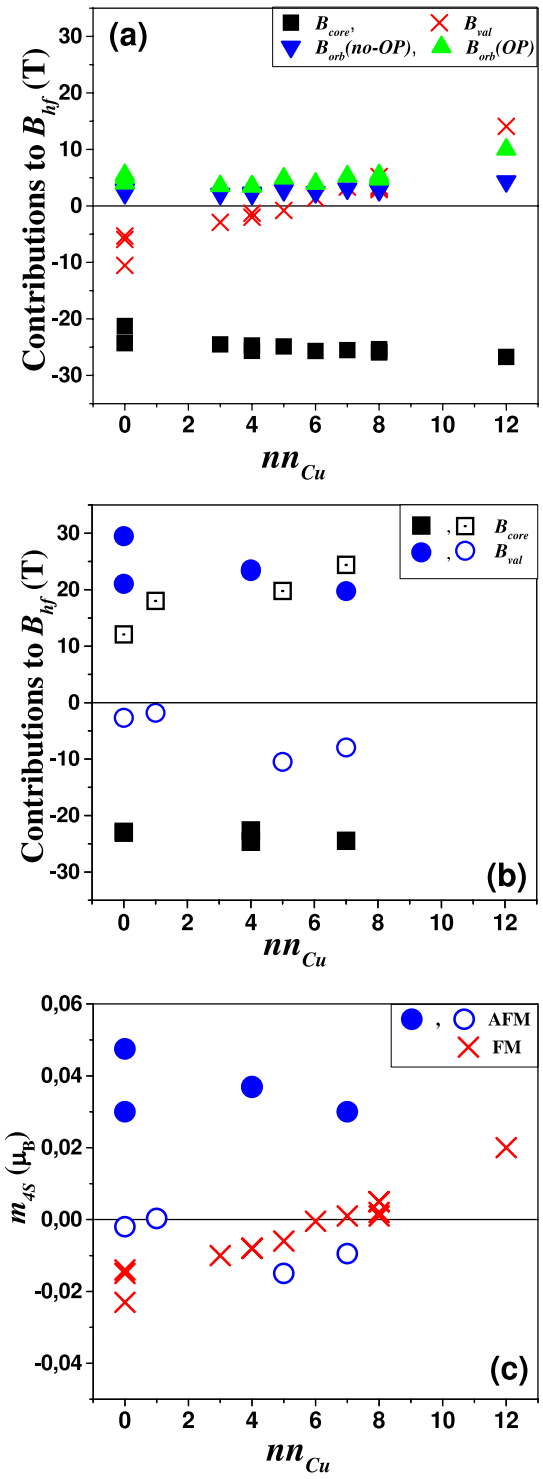

Figure 1. (a) Core (B_{core}), valence (B_{val}) and orbital contributions (B_{orb} (OP) and B_{orb} (no-OP)) to the hyperfine fields at each Fe site as a function of the number of Cu nearest neighbors (nn_{Cu}) in the FM Fe–Cu systems; (b) B_{core} and B_{val} in the AFM Fe–Cu systems; (c) valence s magnetization ($m_{4\mathrm{s}}$) at each Fe site as a function of nn_{Cu} in the FM (crosses) and AFM (open and full circles) Fe–Cu systems. Open and full symbols refer to the two spin directions in the AFM systems.

linear and biunivocal relation between $B_{\rm core}$ and $nn_{\rm Cu}$ in the AFM systems (see figure 1(b)). It is worth remarking that DFT calculations using the LSDA can lead to core hyperfine field constants differing by up to 30% from experiments [74].

The orbital contributions to the hyperfine fields in the FM systems (figure 1(a)) are always positive and, following the m_L trends, exhibit a very small variation with $nn_{\rm Cu}$ towards larger values. Except for the impurity case ($nn_{\rm Cu} = 12$) this very small variation does not affect the $B_{\rm hf}$ trends. In the AFM Fe precipitates, $B_{\rm orb}$ is also proportional to m_L with roughly the same $\alpha_{\rm orb}$ as obtained in the FM cases (see tables 2 and 3). Furthermore, in the FM systems (figure 1(a)) the valence contribution varies almost linearly with $nn_{\rm Cu}$ but is negative for $nn_{\rm Cu} \leqslant 5$ and positive for $nn_{\rm Cu} > 5$. As can be seen in table 3, this $B_{\rm val}$ sign change is also observed in each FM system as we go from the innermost to the outermost shells. On the other hand, $B_{\rm val}$ does not follow such a simple dependence with $nn_{\rm Cu}$ in the AFM systems, as can be easily seen in figure 1(b). To study the behavior of $B_{\rm val}$ at 3d impurities in metallic systems, a model with two terms has been suggested [61]: one proportional to the contribution of the 4s electrons to the local magnetic moment ($m_{4\rm s}$) and the other given by a product involving the 4s occupation and the difference between probabilities of finding 4s electrons of up and down spins at the nucleus. A more direct analysis often used [75] is to assume that $B_{\rm val}$ is simply proportional to $m_{4\rm s}$. To investigate this model, $m_{4\rm s}$ is plotted in figure 1(c) as a function of $nn_{\rm Cu}$. We clearly see the linear correlation between $m_{4\rm s}$ (figure 1(c)) and $B_{\rm val}$ (figures 1(a) and (b)). Finally, we see that $B_{\rm val}$ and $B_{\rm orb}$ are of the same order of magnitude in the FM systems. Therefore, according to the sign of $B_{\rm val}$, the sum $B_{\rm val} + B_{\rm orb}$ and the magnitude of the total hyperfine field are enhanced or diminished but, due to the much larger negative core contributions, $B_{\rm hf}$ remains negative and decreases almost linearly in magnitude with increasing $nn_{\rm Cu}$. This is not the case of the Fe sites in the AFM Fe precipitates (figure 1(b)), where $B_{\rm val}$ is of the same order of $B_{\rm core}$ but with opposite sign, which reduces the magnitude of $B_{\rm hf}$ by several tesla.

In order to investigate the relation between the average Fe hyperfine field ($\bar{B}_{\rm hf}$) and the number of Fe atoms, we present in table 4 the average core ($\bar{B}_{\rm core}$), valence ($\bar{B}_{\rm val}$) and orbital ($\bar{B}_{\rm orb}$) contributions to the $\bar{B}_{\rm hf}$ for each FM system considered here. These $\bar{B}_{\rm hf}$ results (figure 2(a)) and their partial contributions (figure 2(b)) are plotted as a function of the number of Fe atoms in the embedded cluster in figure 2. For the SF Fe37* and AFM systems, the average of the magnitude of the total hyperfine field ($\overline{|B_{\rm hf}|}$) and the average of the magnitude of the Fermi contact hyperfine field ($\overline{|B_{\rm hfc}|}$) were considered in the systematic and shown in table 4. For easy reference (with a usual Mössbauer measurement), these results are plotted in figure 2(a) assuming a negative sign. Considering the FM Fe precipitates and the Fe–Cu alloy clusters (FM and SF) (table 4 and figure 2(a)) we see that, except for the Fe impurity case (representing a very low Fe concentration), the magnitude of $\bar{B}_{\rm hf}$ remains stable, with values $= -20(\pm 2)$ T. As seen from figure 2(b) the three partial contributions are roughly constant in these cases, $\bar{B}_{\rm core}$ and $\bar{B}_{\rm orb}$ scale with the corresponding spin and orbital average magnetic moments and $\bar{B}_{\rm val}$ seems to be more sensitive to the kind of Fe–Cu cluster. The $\bar{B}_{\rm hf}$ in the AFM systems (figure 2(a)) exhibits a different behavior with much smaller magnitudes.

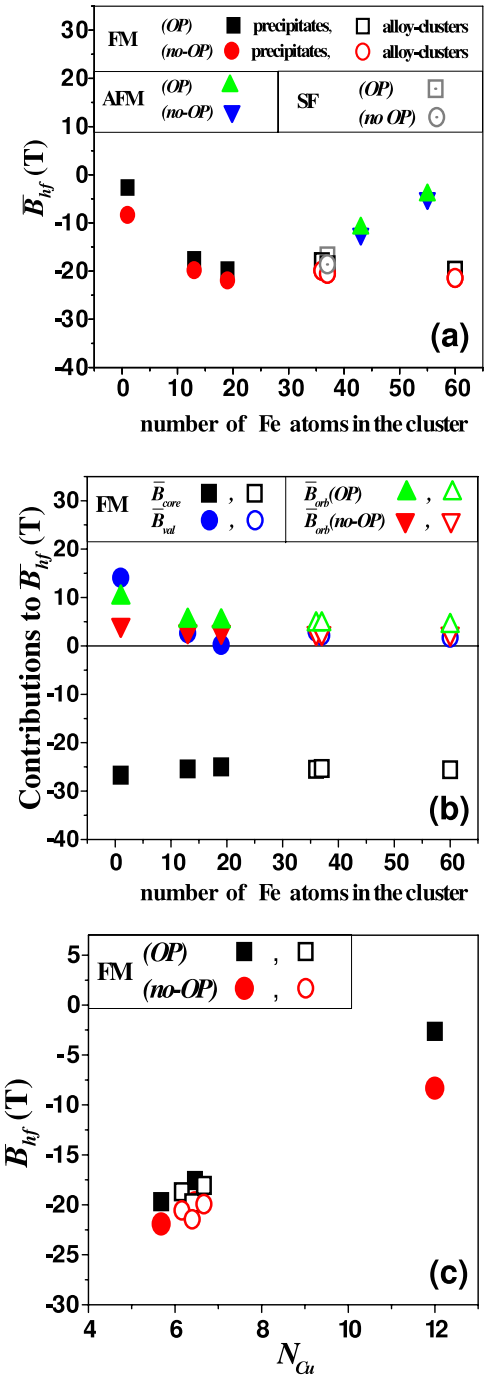

Figure 2. (a) Average hyperfine fields $\bar{B}_{\rm hf}$ as a function of the number of Fe atoms; (b) average core ($\bar{B}_{\rm core}$), valence ($\bar{B}_{\rm val}$) and orbital ($\bar{B}_{\rm orb}$ (OP) and $\bar{B}_{\rm orb}$ (no-OP)) contributions to $\bar{B}_{\rm hf}$ as a function of the number of Fe atoms in the FM Fe–Cu systems; (c) $\bar{B}_{\rm hf}$ as a function of the average number of Cu nearest neighbors ($N_{\rm Cu}$) in the FM Fe–Cu systems. Open symbols refer to FM and SF Fe–Cu alloy clusters and full symbols to FM and AFM Fe precipitates. The calculations are performed with (OP) and without (no-OP) orbital polarization (see text).

Finally, it is also interesting to investigate the correlation between $\bar{B}_{\rm hf}$ and the average number of Cu neighbors ($N_{\rm Cu}$),

Table 4. Average core ($\bar{B}_{\rm core}$), valence ($\bar{B}_{\rm val}$) and orbital ($\bar{B}_{\rm orb}$) contributions to the average hyperfine fields ($\bar{B}_{\rm hf}$) for each FM cluster in Cu. Average of the magnitude of the total hyperfine fields ($\overline{|B_{\rm hf}|}$) and average of the magnitude of the Fermi contact hyperfine fields ($\overline{|B_{\rm hfc}|}$) for each AFM cluster in Cu. Hyperfine fields are in teslas. $N_{\rm Cu}$ and $N_{\rm Fe-AFM}$ are the same as in table 1.

		FM Fe precipitates			Fe–Cu alloy clusters		
		Fe1	Fe13	Fe19	Fe36*	Fe37*	Fe60*
$\bar{B}_{\rm core}$		−26.7	−25.4	−25.0	−25.5	−25.3	−25.6
$\bar{B}_{\rm val}$		14.1	2.6	0.2	3.0	2.1	1.7
$\bar{B}_{\rm orb}$	(No-OP)	4.3	3.0	2.9	2.6	2.6	2.5
	(OP)	10.0	5.2	5.1	4.5	4.5	4.1
$\bar{B}_{\rm hf}$	(No-OP)	−8.3	−19.8	−21.9	−20.0	−20.6	−21.5
	(OP)	−2.6	−17.6	−19.7	−18.1	−18.7	−19.8
$N_{\rm Cu}$		12	6.46	5.68	6.67	6.16	6.4
		AFM Fe precipitates			Fe–Cu alloy clusters		
		Fe43	Fe55		SF Fe37*		
$\overline{\lvert B_{\rm hfc}\rvert}$		13.95	7.3		21.1		
$\overline{\lvert B_{\rm hf}\rvert}$	(No-OP)	12.3	4.9		18.6		
	(OP)	11.1	4.2		16.8		
$N_{\rm Fe-AFM}$		2.8	4.1		0.65		
$N_{\rm Cu}$		4.74	4.15		6.16		

as plotted for the FM systems in figure 2(c). We see a linear decrease in the magnitude of $\bar{B}_{\rm hf}$ with increasing $N_{\rm Cu}$. The variations of the average partial contributions to $\bar{B}_{\rm hf}$ with $N_{\rm Cu}$ (table 4) follow the same trend observed in figure 1(a): (i) $\bar{B}_{\rm core}$ and $\bar{B}_{\rm orb}$ present very small changes except, again, for the impurity case ($N_{\rm Cu} = 12$) and (ii) $\bar{B}_{\rm val}$ exhibits a large variation and is the main factor responsible for the pronounced variation of $\bar{B}_{\rm hf}$ with $N_{\rm Cu}$. This analysis of $\bar{B}_{\rm hf}$ as a function of $N_{\rm Cu}$ in the FM systems presents very interesting results, since $N_{\rm Cu}$ seems to dictate the magnetic moments and hyperfine fields for a given Fe cluster embedded in a Cu host. Nevertheless, if we analyze the results for the SF and AFM systems, shown in table 4, we see that $\overline{|B_{\rm hf}|}$ decreases as a function of increasing $N_{\rm Fe-AFM}$.

3.3.2. Isomer shifts. Experimental IS values plotted as a function of the Fe concentration in Fe–Cu alloys are shown in figure 3(a). Open squares refer to values obtained by MA in [45, 46] and full squares are values for samples prepared by sputtering [3]. Our theoretical IS calculated at the Fe sites in the FM Fe precipitates, AFM Fe precipitates and (FM and SF) Fe–Cu alloy clusters are shown in figure 3(b) as a function of the number of Fe atoms in the embedded cluster. We note that the horizontal axes of figures 3(a) and (b) are not the same, so the magnitude of the IS presented in both figures should not have a one-to-one correspondence. Unfortunately, there is no simple and direct way to correlate the observed nominal Fe concentrations in Fe–Cu alloys with the number of Fe atoms in the theoretical model, since the latter is up to 60 Fe atoms distributed into a region of the order of 1 nm embedded into an fcc Cu lattice with 12 000 atoms. Nevertheless, we can see general trends by comparing the theoretical results with measurements performed at room temperature. We see that the AFM Fe precipitates fit the observed decreasing IS tendency with increasing Fe concentration in samples prepared by sputtering [3]. On the other hand, Fe–Cu alloy clusters (cf figure 3) seem to be better suited to understand the behavior of the IS in the samples obtained by MA [45, 46]. The FM Fe precipitates seem to fit in both models. Sputtering could, instead, present grains of pure metal, similar to the model of the AFM Fe precipitates.

Moreover, the calculated $\bar{B}_{\rm hf}$s (figure 2(a)) also reflect these differences suggested by the ISs. In the AFM Fe precipitates, the magnitudes of $\bar{B}_{\rm hf}$ are around 10 T. These small values correspond to what has been observed (see figure 4 of [3]) for low Fe concentration samples prepared by sputtering (mean values of ∼7 T and ∼8 T at 4.2 K for iron concentrations of 20 at.% and 30 at.%, respectively). The FM Fe precipitates (with up to 19 Fe atoms) and the Fe–Cu alloy cluster systems show a net $\bar{B}_{\rm hf}$ of $-20(\pm 2)$ T. This is in the same range of mean values measured in samples prepared by MA [37, 40, 41, 28, 42–46]. The Schwarz [76] model for MA of Fe–Cu alloys assumes that mutual intermixing between Fe and Cu grains occurs in a two-step process. As a result, Fe-rich grains with Cu impurities, and Cu grains with Fe impurities are formed, in a distribution which resembles the alloy-cluster model. This was already observed through chemical EDS analysis in samples obtained by MA [39, 77]. Also, more recently, measurements for an iron concentration of 23 at.% in an Fe–Cu alloy prepared by MA [37] indicate that this alloy is heterogeneous containing ferromagnetic Fe-rich nanoclusters.

4. Conclusions

We have used the RS-LMTO-ASA scheme to study the local magnetic and hyperfine properties at nanoscopic Fe and Fe–Cu grains in a Cu matrix. The studied Fe–Cu alloy cluster and Fe precipitates with up to 19 Fe atoms are found to order ferromagnetically. For larger precipitates we have found that the moments of Fe atoms at the interface with Cu align parallel

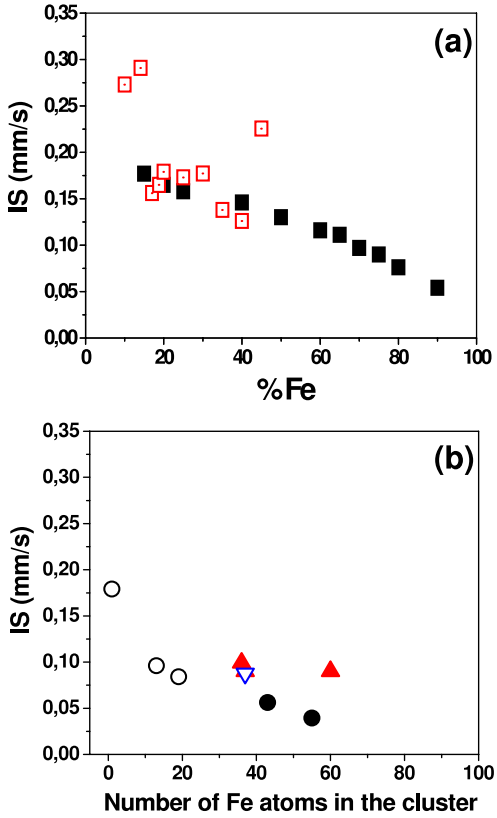

Figure 3. (a) Isomer shifts (IS) measured at the Fe sites in Fe–Cu alloys as a function of the Fe concentration in samples obtained by MA [45, 46] (open squares) and in samples prepared by sputtering [3] (full squares); (b) theoretical IS results in the FM Fe precipitates (open circles), AFM Fe precipitates (full circles) and Fe–Cu alloy clusters (FM: up triangles, SF: down triangle) embedded in Cu. All results are referred to α-Fe.

with each other. Also, the exchange interactions between more distant Fe pairs, located on the same inner shell, present competing values with contributions which approximately cancel each other. The magnetic frustrations obtained for these clusters probably arise as a consequence of these competitions.

Spin and orbital contributions to the local magnetic moments and to the hyperfine fields have been calculated. Although the orbital moments of the Fe atoms are small and remain almost constant regardless of the cluster size, they yield significant orbital contributions to the hyperfine fields. Since these orbital hyperfine fields can be of the same order of magnitude as the valence contributions they cannot be neglected in a systematic study of the behavior of hyperfine fields in Fe–Cu systems. The spin moments at the Fe atoms show an enhancement with increasing number of Cu nearest neighbors in the FM systems. We have shown that the quantities which dictate the magnetic moments and hyperfine fields at the Fe sites in the FM clusters embedded in Cu are the number and, most interesting, the average number of Cu nearest neighbors. We have also studied the average hyperfine field and Mössbauer IS behavior as a function of the number of Fe atoms in the clusters and found different trends in the AFM precipitates and FM alloy clusters. This is mainly due to the different average number of Cu neighbors in the two models. We obtained that both small (up to 19 atoms) FM Fe precipitates and Fe–Cu alloy clusters present average values of the IS in a 'bounded to a given narrow range', as observed in MS measurements for samples obtained by MA. On the other hand, in samples prepared by sputtering, the AFM Fe precipitates should be present, since the theoretical average values of the IS shows the characteristic decreasing tendency with increasing (low) Fe concentration observed by MS in these cases. The relation among these models and the preparation route is also supported by the hyperfine field trends discussed here. Although the Fe content in a given sample cannot be related in a straightforward manner to the number of Fe atoms in the systems we have considered, it can give overall important information about observed trends.

Acknowledgments

This work was supported by FAPESP, FAPESPA, CNPq and Capes and used some computational facilities at CENAPAD-UNICAMP and LCCA-USP obtained within the INEO project and FAPESP (proc. 2004/08928-3). We would like to thank Hercílio R Rechenberg (in memorium) for profitable discussions and S Frota-Pessôa for support with the RS-LMTO-ASA code.

References

[1] Ma E 2005 *Prog. Mater. Sci.* **50** 413
[2] Massalski T B and Okamoto H 1990 *Binary Alloy Phase Diagram* vol 1–3 (Materials Park, OH: ASM International)
[3] Chien C L, Liou S H, Kofalt D, Yu W, Egami T and McGuire T R 1986 *Phys. Rev.* B **33** 3247
[4] Duc N H, Huong Giang D T, Fnidiki A and Teillet J 2003 *J. Magn. Magn. Mater.* **262** 420
[5] Sumiyama K and Nakamura Y 1983 *J. Magn. Magn. Mater.* **35** 219
[6] Uchiyama T, Matsui M and Adachi K 1987 *IEEE Trans. Magn.* **23** 2305
[7] Shingu P H (ed) 1992 *Mechanical Alloying, Materials Science Forum* vol 88–90 (Singapore: Trans Tech Publications)
[8] James P, Eriksson O, Johansson B and Abrikosov I A 1999 *Phys. Rev.* B **59** 419
[9] Mashimo T, Huang X, Fan X, Koyama K and Motokawa M 2002 *Phys. Rev.* B **66** 132407
[10] Gorria P, Martinez-Blanco D, Blanco J A, Hernando A, Garitaonandia J S, Fernandez Barquin L, Campo J and Smith R I 2004 *Phys. Rev.* B **69** 214421
Gorria P, Martinez-Blanco D, Blanco J A, Perez M J, Hernando A, Barquin L F and Smith R I 2005 *Phys. Rev.* B **72** 014401
[11] Khmelevskyi S and Mohn P 2005 *Phys. Rev.* B **71** 144423
[12] Orecchini A, Sacchetti F, Petrillo C, Postorino P, Congeduti A, Giorgetti Ch, Baudelet F and Mazzone G 2006 *J. Alloys Compounds* **424** 27
[13] Bagayoko D and Callaway J 1983 *Phys. Rev.* B **28** 5419
Wright J G 1971 *Phil. Mag.* **24** 217
Gradmann U, Kummerle W and Tillmans P 1976 *Thin Solid Films* **34** 249
[14] Tsunoda Y 1989 *J. Phys.: Condens. Matter* **1** 10427
[15] Naono T and Tsunoda Y 2004 *J. Phys.: Condens. Matter* **16** 7723
[16] Tsunoda Y, Nogami H and Takasaka M 2007 *Phys. Rev.* B **76** 054419
[17] Mryasov O N *et al* 1991 *J. Phys.: Condens. Matter* **3** 7683

[18] Uhl M, Sandratskii L M and Kübler J 1992 *J. Magn. Magn. Mater.* **103** 314
[19] Antropov V P, Katsnelson M I, van Schilfgaarde M and Harmon B N 1995 *Phys. Rev. Lett.* **75** 729
Antropov V P, Katsnelson M I, Harmon B N, van Schilfgaarde M and Kusnezov D 1996 *Phys. Rev.* B **54** 1019
[20] Körling M and Ergon J 1996 *Phys. Rev.* B **54** R8293
[21] Knöpfle K, Sandratskii L M and Kübler J 2000 *Phys. Rev.* B **62** 5564
[22] Kurz Ph, Förster F, Nordström L, Bihlmayer G and Blügel S 2004 *Phys. Rev.* B **69** 024415
[23] Sjöstedt E and Nordström L 2002 *Phys. Rev.* B **66** 014447
[24] Marsman M and Hafner J 2002 *Phys. Rev.* B **66** 224409
[25] Ruban A V, Katsnelson M I, Olovsson W, Simak S I and Abrikosov I A 2005 *Phys. Rev.* B **71** 054402
[26] Abrikosov I A, Kissavos A E, Liot F, Alling B, Simak S I, Peil O and Ruban A V 2007 *Phys. Rev.* B **76** 014434
[27] Shallcross S, Kissavos A E, Sharma S and Meded V 2006 *Phys. Rev.* B **73** 104443
[28] Crespo P, Hernando A, Yavari R, Drbohlav O, García-Escorial A, Barandiarán J M and Orue I 1993 *Phys. Rev.* B **48** 7134
[29] Ma E, Atzmon M and Pinkerton F E 1993 *J. Appl. Phys.* **74** 955
[30] Principi G *et al* 2001 *J. Alloys Compounds* **326** 188
[31] Gong H R, Kong L T and Liu B X 2004 *Phys. Rev.* B **69** 054203
[32] Serena P A and García N 1994 *Phys. Rev.* B **50** 944
[33] Cai J-W *et al* 1992 *J. Phys.: Condens. Matter* **4** 8813
[34] Shingu P H, Ishihara K N, Uenishi K, Kuyama J, Huang B and Nasu S 1990 *Solid State Powder Processing* ed A H Clauer and J J de Barbadillo (Pennsylvania: The Minerals, Metals and Materials Society) p 21
[35] Uenishi K, Kobayashi K, Nasu S, Hatano H, Ishihara K and Shingu P H 1992 *Z. Metallk.* **83** 132
[36] Eckert J, Holzer J C, Krill C E III and Johnson W L 1992 *J. Mater. Res.* **7** 1980
Eckert J, Holzer J C and Johnson W L 1993 *J. Appl. Phys.* **73** 131
[37] Silva N J O, Amaral J S, Amaral V S, Costa B F O and Le Caër G 2009 *J. Phys.: Condens. Matter* **21** 046003
[38] Kravtsova A N, Yalovega G E, Soldatov A V, Yan W S and Wei S Q 2009 *J. Alloys Compounds* **469** 42
[39] Huang J Y, Jiang J Z, Yasuda H and Mori H 1998 *Phys. Rev.* B **58** R11817
[40] Jiang J Z, Gonser U, Gente C and Bormann R 1993 *Appl. Phys. Lett.* **63** 1056
Jiang J Z, Gonser U, Gente C and Bormann R 1993 *Appl. Phys. Lett.* **63** 2768
[41] Macri P P, Rose P, Frattini R, Enzo S, Principi G, Hu W X and Cowlam N 1994 *J. Appl. Phys.* **76** 4061
[42] Ding J, Eilon M, Street R, Pierre T St, Smith P and McCormick P G 1995 *J. Magn. Magn. Mater.* **140–144** 471
[43] Li T, Li Y-Z, Zhang Y-H, Gao C, Wei S-Q and Liu W-H 1995 *Phys. Rev.* B **52** 1120
[44] Monteiro D W L, Larica C, Nunes E, Passamani E C and Alves K M B 1998 *Hyperfine Interact.* C **3** 17–20
[45] Socolovsky L M and Sánchez F H 2004 *J. Metastable Nanocryst. Mater.* **22** 97
[46] Socolovsky L M, Sánchez F H and Shingu P H 2001 *Hyperfine Interact.* **133** 47
[47] Frota-Pessôa S 1992 *Phys. Rev.* B **46** 14570
Peduto P R, Frota-Pessôa S and Methfessel M S 1991 *Phys. Rev.* B **44** 13283
[48] Frota-Pessôa S 2004 *Phys. Rev.* B **69** 104401
[49] Andersen O K 1975 *Phys. Rev.* B **12** 3060
Andersen O K, Jepsen O and Glötzel D 1985 *Highlights of Condensed Matter Theory* (Amsterdam: North-Holland)
[50] Haydock R 1980 *Solid State Physics* vol 35 (New York: Academic) p 215
[51] Brewer W D, Scherz A, Sorg C, Wende H, Baberschke K, Bencok P and Frota-Pessôa S 2004 *Phys. Rev. Lett.* **93** 077205
[52] Nogueira R N and Petrilli H M 2000 *Phys. Rev.* B **63** 012405
[53] Frota-Pessôa S, de Mello L A, Petrilli H M and Klautau A B 1993 *Phys. Rev. Lett.* **71** 4206
Legoas S B and Frota-Pessôa S 2000 *Phys. Rev.* B **61** 12566
Bergman A, Holmström E, Niklasson A M N, Nordström L, Frota-Pessôa S and Eriksson O 2004 *Phys. Rev.* B **70** 174446
[54] Klautau A B, Peduto P R and Frota-Pessôa S 1998 *J. Magn. Magn. Mater.* **186** 223
[55] Legoas S B, Araujo A A, Laks B, Klautau A B and Frota-Pessôa S 2000 *Phys. Rev.* B **61** 10417
[56] Klautau A B and Frota-Pessôa S 2005 *Surf. Sci.* **579** 27
Klautau A B and Frota-Pessôa S 2004 *Phys. Rev.* B **70** 193407
Klautau A B and Frota-Pessôa S 2002 *Surf. Sci.* **497** 385
[57] Frota-Pessôa S, Klautau A B and Legoas S B 2002 *Phys. Rev.* B **66** 132416
Klautau A B, Legoas S B, Muniz R B and Frota-Pessôa S 1999 *Phys. Rev.* B **60** 3421
Eriksson O, Bergqvist L, Holmström E, Bergman A, LeBacq O, Frota-Pessôa S, Hjörvarsson B and Nordström L 2003 *J. Phys.: Condens. Matter* **15** 599
[58] Bergman A, Nordström L, Klautau A B, Frota-Pessôa S and Eriksson O 2006 *Phys. Rev.* B **73** 174434
Bergman A, Nordström L, Klautau A B, Frota-Pessôa S and Eriksson O 2006 *Surf. Sci.* **600** 4838
Bergman A, Nordström L, Klautau A B, Frota-Pessôa S and Eriksson O 2007 *J. Phys.: Condens. Matter* **19** 156226
[59] Eriksson O, Johansson B, Albers R C, Boring A M and Brooks M S S 1990 *Phys. Rev.* B **42** 2707
[60] Brooks M S S 1985 *Physica* B **130** 6
Eriksson O, Brooks M S S and Johansson B 1990 *Phys. Rev.* B **41** 7311
[61] Frota-Pessôa S and Legoas S B 2001 *Hyperfine Interact.* **133** 207
[62] Petrilli H M and Frota-Pessôa S 1993 *Phys. Rev.* B **48** 7148
[63] Kirsch R, Prandolini M J, Beutler O, Brewer W D, Gruyters M, Kapoor J, Riegel D, Ebert H and Frota-Pessôa S 2002 *Europhys. Lett.* **59** 430
[64] Terrazos L A and Frota-Pessôa S 1997 *Phys. Rev.* B **56** 13035
[65] Beer N and Pettifor D G 1984 *The Electronic Structure of Complex Systems* ed W Temmermann and P Phariseau (New York: Plenum)
[66] von Barth V and Hedin L 1972 *J. Phys. C: Solid State Phys.* **5** 1629
[67] Bergman A 2006 *PhD Thesis* Uppsala University http//publications.uu.se/theses/abstract.xsql?dbid=6763
[68] Liechtenstein A I, Katsnelson M I, Antropov V P and Gubanov V A 1987 *J. Magn. Magn. Mater.* **67** 65
[69] Frota-Pessôa S, Muniz R B and Kudrnovsky J 2000 *Phys. Rev.* B **62** 5293
[70] Costa A T, Muniz R B and Mills D L 2005 *Phys. Rev. Lett.* **94** 137203
[71] Drittler B, Ebert H, Zeller R and Dederichs P H 1989 *Phys. Rev.* B **39** 6334
[72] Li Z Q, Hashi Y and Kawazoe Y 1997 *J. Magn. Magn. Mater.* **167** 123
[73] Baker S H, Asaduzzaman A M, Roy M, Gurman S J, Binns C, Blackman J A and Xie Y 2008 *Phys. Rev.* B **78** 014422
[74] Blügel S, Akai H, Zeller R and Dederichs P H 1987 *Phys. Rev.* B **35** 3271
Ebert H, Strange P and Gyorffy B L 1988 *Z. Phys.* B **73** 77
[75] de Oliveira A L, Tovar Costa M V, de Oliveira N A and Troper A 2000 *J. Appl. Phys.* **87** 4882
[76] Schwarz R B 1998 *Mater. Sci. Forum* **269–272** 665
[77] Huang J Y, Wu Y K and Ye H Q 1998 *Microsc. Res. Tech.* **40** 101